First-principles study of the adsorption of Au atoms and Au_2 and Au_4 clusters on FeO/Pt(111)

Runhai Ouyang and Wei-Xue Li*

State Key Laboratory of Catalysis and Center for Theoretical and Computational Chemistry, Dalian Institute of Chemical Physics, Chinese Academy of Sciences, Dalian 116023, China

(Received 30 July 2011; published 4 October 2011)

Adsorption of Au atoms and Au_2 and Au_4 clusters on Pt(111)-supported bilayer FeO film were studied using first-principles density functional theory. For atom adsorption on the FeO/Pt(111) coincidence lattice, two types of adsorption were found, in agreement with previous studies. One is that the Au atom binds with one Fe cation lifted from underneath to the top of the oxygen layer (flipped adsorption), and the other is that the Au atom adsorbs directly on the oxygen layer (direct adsorption). Flipped adsorption was found to be energetically most favored in all domains of the Moiré superstructure, while direct adsorption was either metastable or unstable. The charge of the Au adatom is negative for the flipped adsorption and positive for the direct adsorption. For the Au_2 and Au_4 clusters, the global most stable adsorption configurations on the FeO/Pt(111) were explored, and the results indicated that one-dimensional (dimer) or two-dimensional (Au_4) upright configurations of direct adsorption were energetically preferred over the flat or three-dimensional ones throughout the Moiré superstructure. Moreover, it was found that the configurations of Au_2 dimers and Au_4 clusters on FeO/Pt(111) is tightly related to the interfacial interaction including two effects: the direction-dependent reactivity of a planar Au cluster and the interfacial electrostatic interaction between the Au clusters and the FeO/Pt(111) support. The role of relativistic effects in the configuration of Au clusters and the interaction with FeO/Pt(111) were illustrated. The evolution of small Au cluster configuration on FeO/Pt(111) was discussed.

DOI: 10.1103/PhysRevB.84.165403 PACS number(s): 68.43.−h, 68.47.Jn, 82.65.+r, 73.30.+y

I. INTRODUCTION

Ultrathin oxide film has been attracting considerable research attention due to its unexpected physical and chemical properties, its characterization accessibility by modern surface techniques, and its potential applications in heterogeneous catalysis and many other fields.[1–3] It has been shown that ultrathin oxide films can be used as excellent catalyst support in model catalysis studies because of the advantages of representing part of the complexity in realistic heterogeneous catalysis, as well as the ability of its surface atomic structure and electronic properties to be characterized in detail.[4] By controlling the film thickness or film-metal support interfacial structure and composition, the catalytic activity of the films or supported metal catalysts can further be tuned.[5–7]

Lots of high-quality ultrathin oxide films have been fabricated in experiments so far. In particular, the ultrathin oxide films of stoichiometric and clean polar surfaces, which are unstable for their bulk counterparts, for instance the commonly studied ZnO(0001),[8,9] MgO(111),[10,11] and FeO(111),[12–15] can be well prepared. These perfect polar ultrathin films could stabilize themselves through reducing the anion-cation interlayer distance and interacting with metal substrate, thereby lower the surface dipole.[16–19] In view of the well-defined surface of polar films, they can be used as a polar template to study the physical and chemical properties of supported metal particles or molecules, and catalytic properties.[20–22]

Ever since the discovery of the catalytic activity of a gold nanoparticle supported on oxide,[23,24] the "gold rush" in catalysis research was inspired to try to understand the origin of the particles' abnormal catalytic activity and exploring the potential application in heterogeneous catalysis.[25–27] Many factors, such as particle size, charge transfer, coordination number, and support effects, have been proposed to play a crucial role with regard to the catalytic function of gold nanoparticles.[28–33]

Among others, particle geometry is one of the most studied subjects since it is well related to the particle size and coordination number. The evolution of Au-particle geometry, either in gas phase or on oxide support, has been studied extensively as the Au particle size varies from a single atom to clusters and nanoparticles. In the gas phase, planar configurations were found to be preferred for small Au_n clusters with the transition from two to three dimensions at $n = 13$ for anion,[34] 8 for cation,[35] and 12 for neutral.[36] On oxide support such as the most studied regular MgO(100) surface, the Au atom adsorbs at the O-top site through electrostatic polarization and weak interfacial orbital hybridization, along with large Pauli repulsion.[37–39] For small Au clusters, planar upright configurations have been recognized on MgO(100) surfaces, both from theoretical calculations and experiment.[40–43] Small Au clusters on MgO(100) tend to keep their intrinsic two-dimensional (2D) configurations of the gas phase due to the weak interaction of Au with MgO(100).[34–36] Furthermore, the planar clusters preferred to adopt the upright configuration against the MgO(100) surface because of the relative high reactivity of the Au atoms at regions on the rim of the planar cluster and along the direction of the planar cluster axis.[41,42] On metal-supported ultrathin oxide film, the geometry and charge of Au clusters could be different from those on the surface of bulk counterparts. Charging of the adsorbed particle could be affected by electron tunneling through the oxide film from or to the underlying metal support due to the requirement of Fermi energy alignment or the quasisteady state of the electron flux on the electronic levels between the adsorbate and the substrate.[44,45] Small Au clusters on Ag(100)-supported 2 ML MgO(100) film were negatively charged. For Au atoms, they occupied the hollow site.[39] For Au_2 dimers, they preferred to adopt the upright configuration against the MgO/Mo(100) surface,[46] and for Au_n ($3 \leqslant n \leqslant 7$) clusters, one-dimensional (1D) flat configurations were

preferred.[47] On Mo(100)-supported 2 ML MgO(100) film, 2D flat configurations were preferred for Au_n ($8 \leqslant n \leqslant 20$) clusters.[48]

The interest in understanding how the polarity of ultrathin oxide film affects the structure and charge state of deposited metal particles prompted us to investigate the Au atom and small cluster adsorption on the perfect FeO/Pt(111) polar surface. FeO/Pt(111) is a well-studied system and was found to be an important model system for supported catalysts.[5] The adsorption of Au atoms and small clusters on polar FeO film at low temperature has been investigated by experiment,[21,22,49] and it was found that Au atoms or small clusters primarily occupy a specific domain of the Moiré superstructure.[21,49] Moreover, the differential conductance spectroscopy on Au adatoms showed a peak at 0.5 V for those in the highly populated domain and no peak around 0.5 V for those in the other domains, which indicated different adsorption configurations.[21] Positively charged Au adatoms were inferred from the adsorption of the probe molecule CO, combining scanning tunneling microscopy (STM) and theoretical calculations.[49] Furthermore, theoretical calculations predicted another type of Au adatom binding with a lifted low-lying Fe cation and negatively charged.[49,50] However, the negatively charged Au adatom was not observed by the experiment.[49] Thus whether the negative Au adatoms exist is yet not certain, partly because the theoretical prediction was based on the use of a reduced nonpseudomorphic calculation model to simulate the Moiré superstructure of FeO/Pt(111).[49] The adsorption of small Au clusters on the MgO(100) surface was well studied and understood; however, which is the preferred configuration and charge state on a perfect polar surface like FeO/Pt(111) is still awaiting exploration.

To address these questions, we employed density functional theory (DFT) to investigate the adsorption structure and corresponding charge of Au atoms, Au_2, and Au_4 clusters on Pt(111)-supported bilayer FeO film with a realistic model (without statement otherwise) of the Moiré superstructure observed by experiment.[12] In Sec. II, the methods and computational details are described. In Sec. III, the results of Au atom adsorption are presented, followed by the study of Au cluster adsorption.

II. METHODS AND COMPUTATIONAL DETAILS

DFT calculations were carried out using the Vienna Ab Initio Simulation Package (VASP),[51] in which the core-valence electron interaction was described by projector augmented wave.[52] The calculations were performed at the DFT + U level with $U = 4$ and $J = 1$ for iron,[53,54] using the generalized-gradient approximation and the Perdew-Wang functional.[55] The initial magnetic structures of bilayer FeO were set to be antiferromagnetic.[54] The wave function was expanded by a plane wave with cutoff energy 350 eV, and a single k-point for Brillouin zone sampling. The FeO/Pt(111) surface was simulated using the measured superstructure $(\sqrt{84} \times \sqrt{84})R \times 10.9^\circ$-FeO/Pt(111) of the FeO coverage $\Theta_{\mathrm{FeO}} < 1$ ML,[12] in which the FeO bilayer was supported on a three-layer Pt slab. All atoms were allowed to fully relax until the residual force was less than 0.03 eV/Å, except for the bottom two Pt layers fixed to bulk truncated positions. The barriers were calculated using the climbing image nudged elastic band method[56] with a total of five images including the end points.

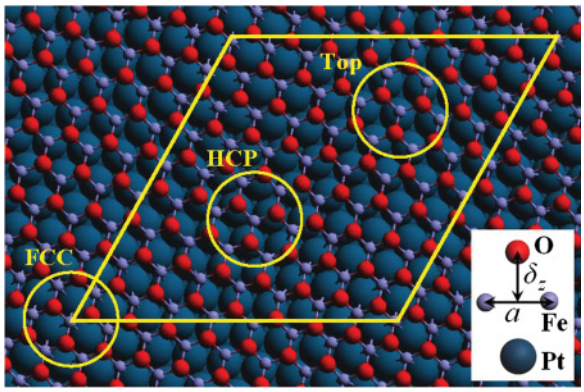

FIG. 1. (Color online) The Moiré superstructure of the FeO/Pt(111) coincidence lattice. Three domains, FCC, HCP, and Top are indicated. Large (cyan) spheres, Pt atoms; medium (red) spheres, O atoms; small (blue) spheres, Fe atoms; δ_z, Fe-O layer distance or rumpling (Å); a, Fe-Fe distance or in-plane lattice parameter (Å).

III. RESULTS AND DISCUSSION

A. Structure and electronic properties of FeO/Pt(111)

Due to the lattice mismatch between the grown bilayer FeO(111) film (3.10 Å) and the Pt(111) (2.77 Å) substrate, a Moiré superstructure with periodicity of 25.4 Å was created when the coverage of FeO was less than one monolayer.[12] There are three domains inside the Moiré superstructure: FCC (Fe atoms occupy fcc sites of Pt(111) surface), HCP (Fe atoms occupy hcp sites), and Top (Fe atoms occupy top sites), which are shown in Fig. 1. O atoms in all domains sit on the Fe layer and follow the fcc stacking sequence. Calculated structural and electronic properties of the three domains and cell average are summarized in Table I. The domain properties are averaged using the central seven FeO formula of each domain as the circles indicate in Fig. 1.

For the cell average, the calculated in-plane lattice constant of FeO, a, is 3.10 Å, the interface distance between FeO and Pt, $z_{\mathrm{FeO\text{-}Pt}}$, is 2.67 Å, the Fe-O rumpling δ_z is 0.68 Å, and the surface electrostatic potential δV at a height of 4.4 Å from each of the surface O atoms is 5.77 eV with respect to the Fermi level. In addition, the calculated interfacial adhesion

TABLE I. Calculated structural and electronic properties on the FCC, HCP, and Top domains and cell averages of FeO/Pt(111).[a]

Domain	a (Å)	$z_{\mathrm{FeO\text{-}Pt}}$ (Å)	δ_z (Å)	δV (eV)
Average	3.10	2.67	0.68	0.00(5.77)
FCC	3.01	2.61	0.76	0.23(6.00)
HCP	3.10	2.62	0.70	0.00(5.77)
Top	3.16	2.77	0.56	−0.27(5.50)

[a] a is the in-plane FeO lattice parameter; $z_{\mathrm{FeO\text{-}Pt}} = (z_{\mathrm{Fe}} + z_{\mathrm{O}})/2 - z_{\mathrm{Pt}}$ is the interface distance of FeO with respect to the Pt substrate; $\delta_z = z_{\mathrm{O}} - z_{\mathrm{Fe}}$ is the Fe-O rumpling; δV is the surface electrostatic potential at a height of 4.4 Å from each of the surface O atoms referencing the cell average (referencing the Fermi energy).

TABLE II. Calculated Au-atom adsorption sites (the names beginning with "O" belong to direct adsorption, while those with "Fe" belong to flipped adsorption), adsorption energy (eV), Bader charge ($|e|$), and Au-O or Au-Fe bond length (Å).

Domain	FCC			HCP			Top		
Initial configuration	O-fcc	O-hcp	O-top	O-fcc	O-hcp	O-top	O-fcc	O-hcp	O-top
Optimized configuration	O-top	O-top (Fe-top[a])	O-top	O-top	Fe-top	O-top	Fe-bridge	Fe-top	Fe-top
Adsorption energy		−0.71 (−0.89)		−0.63	−1.00		−0.56	−0.93	
Bader charge		+0.40 (−0.33)		+0.29	−0.33		−0.30	−0.33	
Bond length		2.08 (2.39)		2.09	2.42		2.72, 2.69	2.42	

[a]The low-lying Fe cannot be lifted automatically by an Au adatom due to kinetic hindrance, and was lifted manually.

energy [the energy difference of FeO/Pt(111) subtracting the isolated freezing structure of FeO and Pt(111) in FeO/Pt(111)] is 1.40 eV/FeO. The charge transfer occurs from FeO to the Pt substrate with each surface Pt atom obtaining $0.27|e|$ on average. For the FCC domain, it has the shortest interface distance $z_{\text{FeO-Pt}}$ of 2.61 Å, which is in line with the strongest interfacial interaction of this domain between the FeO film and the Pt substrate.[57] In addition, the FCC domain has the smallest in-plane lattice parameter a of 3.01 Å, the largest Fe-O rumpling δ_z of 0.76 Å, and the largest local surface electrostatic potential δV of 6.00 eV. The HCP domain has medium values similar to the cell average, while the Top domain has the largest interface distance $z_{\text{FeO-Pt}}$ of 2.77 Å, the smallest Fe-O rumpling δ_z of 0.56 Å, and the lowest surface electrostatic potential δV of 5.50 eV. The smaller the in-plane lattice parameter, the larger the Fe-O rumpling δ_z and the larger the Fe-O dipole strength and surface potential of δV will be.[58] These results are well in agreement with previous experiments[12] and calculations.[59,60]

B. Adsorption of Au atom on FeO/Pt(111)

Calculations of Au atom adsorption on FeO/Pt(111) were performed in all three domains, FCC, HCP, and Top. In each domain, Au-atom adsorption was investigated at three types of site, O-fcc (the center of three O and three Fe atoms), O-hcp (the center of three O atoms and the top of one Fe atom), and O-top, in order to find the most stable configuration. We found there were two types of adsorption. First, the Au atom lifts the low-lying Fe cation and coordinates directly with the lifted Fe cation (so-called flipped adsorption[50]). Accordingly, the Au atom is negatively charged (see Fig. 2). Second, the Au atom binds directly with the oxygen atom (direct adsorption) and is positively charged. The adsorption strength of Au was evaluated by adsorption energy with respect to an Au atom in gas phase and the FeO/Pt(111). The more negative the adsorption energy, the stronger the adsorption is.

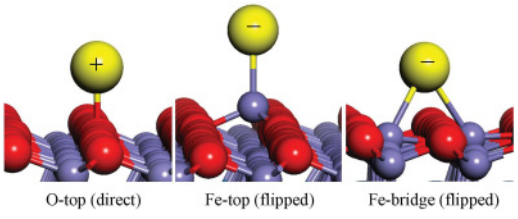

FIG. 2. (Color online) The calculated three typical adsorption sites (type): large sphere (yellow), Au atom; medium (red) spheres, O atoms; and small (blue) spheres, Fe atoms. The sign of the Au adatom charge is indicated on the Au atoms.

In the FCC domain, only direct adsorption was found and was only stable at the O-top site with adsorption energy −0.71 eV and Bader charge $+0.40|e|$ as shown in Table II. The Au atoms initially put at O-hcp and O-fcc sites were relaxed automatically onto the O-top site. In the HCP domain, both direct and flipped adsorptions were found. The Au atoms initially put at O-top and O-fcc sites were relaxed onto the O-top site of direct adsorption with adsorption energy −0.63 eV and Bader charge $+0.29|e|$. The one of Au initially put at the O-hcp site was relaxed automatically onto the Fe-top site of flipped adsorption with one low-lying Fe cation lifted above the oxygen layer spontaneously; the adsorption energy of the Au adatom is −1.00 eV with the Bader charge $-0.33|e|$ as summarized in Table II. In the Top domain, only flipped adsorption was found. The ones initially put at O-top and O-hcp sites were relaxed automatically onto the Fe-top site (for Au at O-top, it first slips onto the O-hcp site, then lifts the low-lying Fe cation) with Au adatom adsorption energy of −0.93 eV and Bader charge $-0.33|e|$. The Au initially put at the O-fcc site lifted two low-lying Fe cations. However, the adsorption energy was only −0.56 eV due to the large deformation of the FeO film.

Thus, the calculations indicate that the most stable adsorption in the HCP and Top domains is the Au adatom on the Fe-top site of flipped adsorption, forming an Au anion with zero barrier. In the FCC domain, a low-lying Fe cation cannot be lifted automatically and the barrier of the Au adatom transiting from the O-top site of direct adsorption onto the adjacent Fe-top site of flipped adsorption was calculated to be 0.39 eV. Therefore, the Au cation at the O-top site of the FCC domain is metastable and will transit into an Au anion at the Fe-top site by passing through a barrier of 0.39 eV. The bond length on average of different domains is 2.09 Å for the Au-O bond at the O-top site, 2.41 Å for the Au-Fe bond at the Fe-top site, and 2.71 Å for the Au-Fe bond at the Fe-bridge site.

Charging and adsorption energy of Au adatoms is correlative with the type of adsorption and the domain characteristic. For the direct adsorption at the O-top site, Au lost its 6s electron, forming an Au cation in order to reduce the surface dipole of FeO pointing toward the support. The larger the surface dipole, the more electrons Au will lose. Since the order of domain rumpling, δ_z, is $\delta_z^{\text{FCC}} > \delta_z^{\text{HCP}} > \delta_z^{\text{Top}}$, the order of the surface dipole in the three domains is the same, which

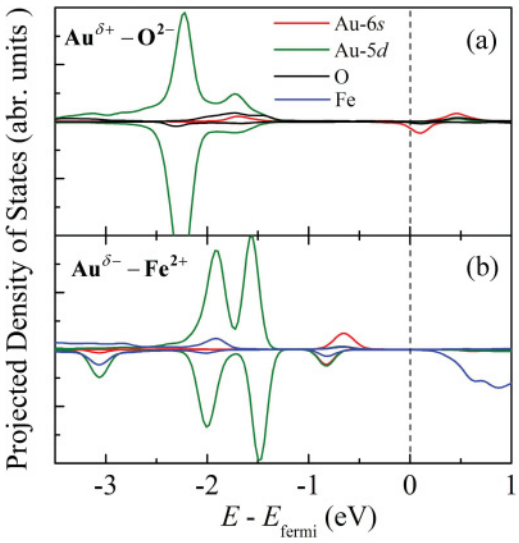

FIG. 3. (Color online) Density of states projected on Au and the bonded O or Fe atoms of the FCC domain: (a) interaction of $Au^{\delta+}$ with O^{2-} at the O-top site, (b) interaction of $Au^{\delta-}$ with Fe^{2+} at Fe-top site.

explains why the charge of an Au adatom at the O-top site in the FCC domain is larger than that in the HCP domain with $+0.40|e|$ and $+0.29|e|$, respectively. Accordingly, the electrostatic interaction for an Au atom at the O-top site will be stronger in the FCC domain than in the HCP domain. Charging of the Au adatom at the O-top site can also be recognized from the projected density of states. It can be seen from Fig. 3(a) that the two 6*s* orbitals of the Au adatom at the O-top site of the FCC domain lie above the Fermi level, which indicates positive charging of the Au adatom with the 6*s* electron lost to the substrate. In addition, we see only weak orbital hybridization between Au and O atoms and thus Au-atom adsorption is mainly contributed by electrostatic interaction. For the flipped adsorption of Au at the Fe-top site, Au formed a strong chemical bond with the lifted Fe cation. As indicated in Fig. 3(b), there is a strong orbital hybridization between the 6*s* and 5*d* orbitals of the Au adatom at the Fe-top site of the FCC domain and the orbitals of the lifted Fe cation, which manifests a strong chemical bond. In addition, the two 6*s* orbitals of the Au adatom are filled, indicating negative charging of the Au adatom.

We note that in the process of Au lifting the low-lying Fe cation, it has to pass the center of three oxygen atoms from underneath to top of the oxygen layer. Thus the larger the in-plane lattice parameter (or the adjacent O-O distance) of FeO, the easier it is for Au to lift out of the low-lying Fe cation. Since the order of the lattice parameter of FeO, a, is $a^{\mathrm{FCC}} < a^{\mathrm{HCP}} < a^{\mathrm{Top}}$, it is understandable as our results indicate that the Au adatom could lift the low-lying Fe cation in the HCP and Top domains automatically, even though no stable direct adsorption of the Au adatom could be found in the Top domain, while this does not happen in the FCC domian. The deformation of FeO film by Au-adatom flipped adsorption is compensated by the strong Au-Fe chemical bond. For instance, the deformation energy of FeO/Pt(111) with one flipped Fe cation lifted by the Au adatom in the HCP domain was calculated to be 0.65 eV, whereas the binding energy of $Au-Fe^{2+}$ was -1.65 eV. It is therefore the flipped adsorption of Au at the Fe-top site of the HCP domain with an adsorption energy of -1.00 eV that is still favored over those of direct adsorption.

In the literature, Au adatoms on FeO/Pt(111) were studied by STM.[21,49] It was concluded that Au adatoms highly populated the HCP domain, and the existence of positively charged Au adatoms was confirmed by combining the experiment of STM and scanning tunneling spectroscopy with DFT calculations. However, some questions remain concerning the adsorption of Au adatoms on FeO/Pt(111). First, DFT calculations with a reduced nonpseudomorphic model of $(\sqrt{7}\times\sqrt{7})R\times19^{o}$-FeO(111)/(3 × 3) Pt(111)[49] or $(\sqrt{3}\times\sqrt{3})R\times30^{o}$-FeO(111)/(2 × 2) Pt(111)[50] predicted another adsorption configuration of Au-atom binding with lifted Fe cation and was negatively charged. However, negative Au adatoms were not detected in the experiment.[49] Whether the Au anion does really exist is still a source of confusion, partly due to the difficulty of calculation using a reduced nonpseudomorphic model to simulate the Moiré superstructure of FeO/Pt(111).[50] Second, whether the highly populated domain is FCC or HCP remains elusive, since the assignment of the two domains, FCC and HCP, from STM is still in debate.[21,49,57–60]

In this work, our nonpseudomorphic calculations using realistic Moiré superstructure indicated that negatively charged Au adatoms of flipped adsorption are energetically preferred and there was no barrier to prevent its formation in the HCP and Top domains. Metastable positively charged Au adatoms of direct adsorption are only possible in the FCC domain, and they could transit into negatively charged Au adatoms of flipped adsorption by overcoming a barrier of 0.39 eV. Considering the order of the surface potential δ_V is $\delta_V^{\mathrm{FCC}} > \delta_V^{\mathrm{HCP}} > \delta_V^{\mathrm{Top}}$, our results support the conclusion about the assignment of the three domains, FCC, HCP, and Top, in the STM image in Refs. 57,59, and 60, and therefore the highly populated domain by Au adatoms should be FCC instead of HCP proposed in Ref. 21. Notice that the differential conductance spectroscopy at 10 K on the Au adatom shows a peak at 0.5 V in the highly populated domain[21]; our results suggest that these Au adatoms may be the metastable Au cation of the FCC domain with the 6*s* electron lost to the substrate and the empty 6*s* orbitals reflected in the differential conductance spectroscopy peak at 0.5 V. The metastable Au cations at the O-top site in the FCC domain can be stable at ultralow temperature, since there is a 0.39-eV barrier before the Au cation transiting into the Au anion. For instance, the transition probability at 50 K is as low as 5.3×10^{-27} estimated from the Arrhenius equation $A\exp(-E/kT)$ with $A = 10^{13}$. Furthermore, no differential conductance spectroscopy peak at 0.5 V was observed on bare oxide film and Au adatoms in other domains.[21] Since our results in Fig. 3 indicate that the 6*s* orbitals of the Au anion are below the Fermi energy and thus there are no empty states of the Au adatom above the Fermi energy and below 1 eV, we suggest these experimentally observed adatoms with no peak at 0.5 V in the conductance spectroscopy may be the Au anions of flipped adsorption at the Fe-top sites in the HCP and Top domains.

C. Adsorption of Au_2 and Au_4 clusters on FeO/Pt(111)

1. Geometry of Au_2 and Au_4 clusters on FeO/Pt(111)

The adsorption of Au_2 and Au_4 clusters, with all possible configurations including the direct and flipped configurations (Fe atoms were manually lifted above oxygen layer), on FeO/Pt(111) were calculated in the FCC and Top domains, which have the largest and smallest local Fe-O rumpling or surface dipole, respectively. The stability of an Au_n cluster was evaluated by the formation energy E_f, defined as $E_f = E(Au_n/FeO/Pt(111)) - E(FeO/Pt(111)) - nE(Au\ atom\ in\ gas)$. For a given number of Au atoms, the more negative the value of E_f, the more stable the Au_n cluster will be. The most stable adsorption structures, as well as some selected metastable ones for comparison, and the corresponding charges of Au_2 and Au_4 clusters are shown in Fig. 4.

In the FCC domain, all atoms of Au_2 and Au_4 adopt direct adsorption with each interfacial Au atom coordinated with one oxygen atom at the O-top site. For the Au_2 dimer, the upright configuration has the lowest formation energy of -3.08 eV and is more stable than the flat configuration (-2.50 eV). The average Bader charge of interfacial Au atoms is $+0.28|e|$ for the upright one and $+0.19|e|$ for the flat one. For the Au_4 cluster, the 2D upright configuration has the lowest formation energy of -7.24 eV, which is more stable than the three-dimensional (3D) tetrahedron configuration of -7.15 eV and the 2D flat configuration of -6.28 eV. In fact, the 2D flat

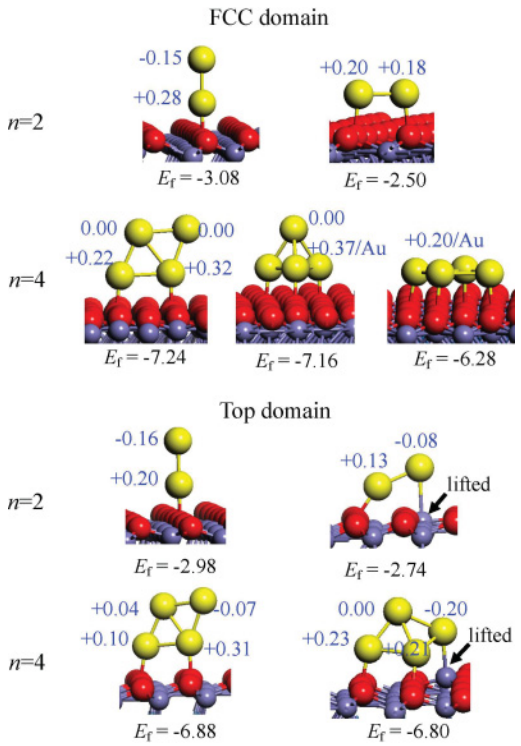

FIG. 4. (Color online) Formation energy (eV) of the most stable and selected metastable configurations of Au_2 and Au_4 clusters in the FCC and Top domains. Numbers beside the Au atoms are their corresponding charge. Large (yellow) spheres, Au atoms; medium (red) spheres, O atoms; small (blue) spheres, Fe atoms. Lifted Fe atoms are indicated by arrows.

Au_4 cluster is unstable in all domains considered and will automatically relax into a 3D configuration. Actually, the 2D flat Au_4 cluster in the FCC domain discussed corresponds to the structure at the transition point from two to three dimensions during the optimization. The average Bader charge of interfacial Au atoms is $+0.27|e|$ for the 2D upright configuration, $+0.37|e|$ for the 3D tetrahedron, and $+0.20|e|$ for the 2D flat configuration.

In the Top domain, the upright Au_2 and Au_4 clusters are of direct adsorption with each interfacial Au atom at the O-top site, as indicated in Fig. 4. For the quasiflat Au_2 and tetrahedral Au_4 clusters on the right side, they each have one interfacial Au atom coordinated with one lifted Fe cation and other interfacial atoms at the quasi-O-top site. For the Au_2 dimer, the upright configuration has the lowest formation energy of -2.98 eV and is more stable than the quasiflat configuration of -2.74 eV. The Bader charge on the interfacial Au atom of the upright configuration is $+0.20|e|$. On the Au atoms of the quasiflat configuration, the one coordinated with the O anion is $+0.13|e|$ and the one coordinated with the Fe cation is $-0.08|e|$. For the Au_4 cluster, the 2D upright configuration has the lowest formation energy of -6.88 eV, which is more stable than the 3D tetrahedron configuration of -6.80 eV. The average Bader charge on the interfacial Au atoms is $+0.21|e|$ for the 2D upright configuration. For the Au atoms of the tetrahedron configuration, the ones coordinated with the O anion have a Bader charge of $+0.22|e|$ and the one coordinated with the Fe cation is $-0.20|e|$. Compared with the upright configurations of Au_2 and Au_4 in the FCC domain, the corresponding ones in the Top domain are less stable, which is due to less interfacial charge on Au clusters in the Top domain and thus weaker interfacial electrostatic interaction.

In both the FCC and the Top domains, our results show that all the considered flipped adsorptions were energetically not preferred. In the Top domain of Fig. 4, the two metastable clusters shown on the right-hand side are of the most energetically preferred configurations among those that have Au atoms of flipped adsorption, which are still less stable than the ones of direct adsorption on the left-hand side. The reason may be that, due to the formation of a strong Au-Au bond, the Au-Fe bond is weakened and thus the advantage of compensating the deformation energy of the lifted Fe cation by forming an Au-Fe bond is no longer present.

The above results indicate that, throughout the FeO/Pt(111) superstructure, the energetically favored configuration of the Au_2 dimer and the Au_4 cluster are 1D (dimer) and 2D (Au_4) upright, respectively. However, the 3D tetrahedron configuration of the Au_4 cluster in either the FCC or the Top domain has a formation energy very close to that of the upright configuration, which suggests that the 3D Au_n cluster on FeO/Pt(111) may be energetically favorable over 2D structures when $n > 4$. In addition, we had also calculated the 2D flat configuration of Au_8 in the FCC domain and the results show it was unstable and relaxed automatically into a 3D structure. These results show clearly that wetting of Au clusters at any size on FeO/Pt(111) was energetically not favored.

2. Origin of the stability of 1D (dimer) or 2D (Au_4) upright configurations

Why would the upright configuration of Au_2 and Au_4 clusters be the preferential structures? We first figure out why the upright configurations on FeO/Pt(111) are preferred over the flat; then we discuss the preference of the 2D upright Au_4 cluster over the 3D tetrahedron.

2D upright over 2D flat. The adsorption of Au_2 and Au_4 clusters could be decomposed into two steps: isolated Au clusters are formed [assuming the optimized structure of an Au cluster on FeO/Pt(111)] from single atoms in gas phase with energy gain E_c, then the clusters adsorb freezingly onto the FeO/Pt(111) surface with interfacial binding energy E_b. Thus the formation energy is $E_f = E_c + E_b$, and the calculated energetics in the FCC domain are shown in Table III. In comparison between the upright and flat configurations for both Au_2 and Au_4, it is clear that E_c are close, while much difference occurs in the quantity of E_b. Therefore, cohesive energy for the upright and flat configurations are similar for either Au_2 or Au_4 clusters, while the upright configurations of Au_2 or Au_4 have a much stronger interfacial interaction than that of the flat configurations. In addition, the interfacial distance of the Au clusters with respect to FeO/Pt(111) for the upright clusters are shorter than those of the flat configuration as shown in Table III, again manifesting stronger interfacial interaction than the upright ones. Therefore, the reason why upright Au_2 and Au_4 configurations are more stable than the corresponding flat ones is that upright Au_2 and Au_4 configurations have stronger interfacial interaction with the FeO/Pt(111) substrate. The Au-Au bond lengths in Au_4 clusters are different and range from 2.60 to 2.80 Å. However, we found that Au-Au bond energy is insensitive to Au-Au bond length; each bond energy difference of Au_4 in gas phase is within 0.05 eV when the bond lengths vary from 2.60 to 2.80 Å.

To see further why the upright clusters on FeO/Pt(111) are more stable than the flat ones, the charge density difference of Au_n/FeO/Pt(111), subtracting the Au_n and FeO/Pt(111) with their atoms assumed at positions of optimized Au_n/FeO/Pt(111) structure, was calculated and is shown in Fig. 5. Stronger charge accumulation in the interface is seen clearly for the upright configuration compared to that of the flat one, which demonstrates the stronger interfacial interaction of the upright configuration with FeO/Pt(111).

The main contribution to the interfacial interaction of Au clusters on FeO/Pt(111) consists of two aspects: the chemical reactivity of Au clusters and the electrostatic interaction between Au clusters and the substrate. The larger the contact area, the larger the interfacial electrostatic interaction will be. The preferred upright configuration must be accompanied by larger chemical reactivity of Au clusters to compensate for the weaker interfacial electrostatic interaction than that of the flat configuration. That is, the reactivity of the Au clusters is direction dependent and the direction along the planar cluster axis is more reactive than the direction perpendicular to the 2D cluster plane or 1D axis. As a result, the configuration of Au clusters on FeO/Pt(111) was determined by two effects: the direction-dependent reactivity of Au clusters and interfacial electrostatic interaction. The first effect would favor the upright configuration, whereas the second effect favors the flat configuration. The former effect overcomes the latter one, and thus the upright configuration is preferred for both Au_2 and Au_4 clusters on FeO/Pt(111).

TABLE III. Energetics and interfacial structure parameters of Au clusters of the FCC domain.

Geometry	E_f (eV)	E_c (eV)	E_b (eV)	z[a] (Å)
Au_2-flat	−2.50	−2.28	−0.22	2.31
Au_2-upright	−3.08	−2.30	−0.78	2.13
Au_4-flat	−6.28	−6.12	−0.16	2.38
Au_4-upright	−7.24	−5.96	−1.28	2.16
Au_4-tetrahedron	−7.15	−4.88	−2.27	2.16

[a]z is the average interface distance of interfacial atoms of the Au cluster with respect to FeO/Pt(111).

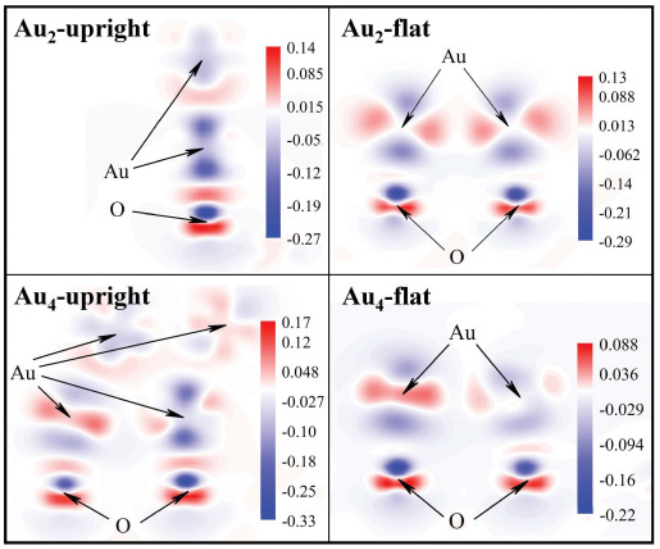

FIG. 5. (Color online) Charge density difference ($n(e)/Å^3$) of upright and flat clusters of Au_2 or Au_4 in the FCC domain. The positions of atoms are indicated at the ends of the arrows. Positive value denotes an increment of electron number.

In order to see whether the relative stability of the upright and flat configurations could be tuned by changing the relative contributions of the two effects, additional comparative calculations of Au_2 and Au_4 clusters on FeO/Pt(111) either with scalar relativistic (SR) or nonrelativistic (NR) effects were carried out. Since the significant relativistic effects on gold led to its high reactivity by strong 6*s*-5*d* orbital hybridization, lower reactivity of Au will occur if the relativistic effects are removed.[61,62] Therefore, the relative magnitude of the two effects of direction-dependent reactivity and interfacial electrostatic interaction of Au clusters on FeO/Pt(111) can be changed in the SR to NR calculations, and so is the relative stability of the upright over the flat geometry.

In this calculation, the FeO/Pt(111) coincidence lattice was simulated by a model of (3×3)-FeO/(3×3)-Pt(111) with FeO in-plane lattice 3.10 Å and Pt lattice expanded to adapt to that of FeO. All Fe atoms sit on the fcc sites of the Pt(111) surface. The DFT code PWSCF[63] was employed, using Vanderbilt ultrasoft pseudopotentials[64] with or

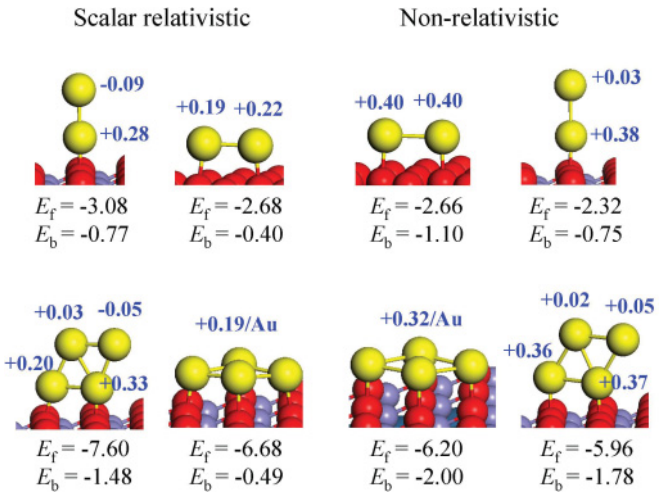

FIG. 6. (Color online) Comparison of stability of upright with flat configuration of Au_2 and Au_4 on FeO/Pt(111) calculated either with or without scalar relativity effect. The Bader charge is shown beside each Au atom, and the formation energy E_f and binding energy E_b of Au clusters were indicated under each structure image.

without the scalar relativity effect to describe the core-valence electron interaction, the Perdew-Wang generalized gradient approximation[55] functional for the exchange-correlation energy, 30 Ry for the plane-wave kinetic energy cutoff, and a $3 \times 3 \times 1$ Monkhorst-Pack[65] k-point grid to sample the Brillouin zone. The on-site Coulomb repulsion was corrected for Fe with $U_{\text{eff}} = 3$.[53,54] All the FeO and the top-layer Pt atoms were allowed to fully relax until the residual force on each atom was less than 0.03 eV/Å, while the bottom two layers of Pt atoms were fixed to the bulk truncated positions.

Calculated results are shown in Fig. 6. In the SR calculations, formation energies E_f for the upright Au_2 and Au_4 configurations are -3.08 and -7.60 eV, respectively, while for the flat Au_2 and Au_4 configurations they are -2.68 and -6.68 eV, respectively. The results agree well with above calculations using realistic superstructure and the VASP code, namely the upright configurations are more stable than the flat ones. In the NR calculations, however, the relative stability is reversed. The formation energies E_f for the upright Au_2 and Au_4 configurations are -2.32 and -5.96 eV, respectively, while those for the flat Au_2 and Au_4 configurations are -2.66 and -6.20 eV, respectively. The flat configurations are more stable than the upright ones. On the one hand, we see from Fig. 6 that charges of interfacial contacted Au atoms are all larger in the NR calculation than in the SR calculation, which enhances the effect of interfacial electrostatic interaction. On the other hand, comparing the upright Au_2 dimer in the NR calculation with that of the SR, their binding energies E_b are almost equal. Given that the interfacial electrostatic interaction in the NR calculation is larger than that of the SR calculation, the reactivity of the Au_2 dimer will be weaker in the NR calculation than in the SR calculation. Thus in the NR calculations, with the effect of direction-dependent reactivity weakened and the effect of electrostatic interaction enhanced, the flat configurations of Au_2 and Au_4 clusters are more stable than the upright ones. These results not only show the importance of relativistic effects on the configuration of Au clusters and the interaction with FeO/Pt(111), but also demonstrate that the configuration of planar Au clusters on FeO/Pt(111) was indeed determined by the two effects, direction-dependent reactivity and interfacial electrostatic interaction.

The two competing effects have also been found for Au cluster adsorption on other oxide supports. Previous study on the chemical properties of small Au clusters shows that planar Au cluster reactivity occurs at regions on the rim and along the direction of the planar cluster axis, an effect favoring upright geometries on perfect oxide substrates such as MgO(100) and anatase TiO_2(101).[42] On the other hand, flat planar Au clusters on Mo(100)-supported thin MgO film have been found to be preferential due to the large electron transfer from metal Mo to the Au cluster and thus the strong interfacial electrostatic interaction,[48] an effect favoring flat geometries. Therefore, whether a small planar Au cluster prefers a flat or upright configuration is tightly related to the oxide supports.

2D upright over 3D tetrahedron. As Table III indicated, the cohesive energy E_c is -5.96 eV for the Au_4 upright configuration and -4.88 eV for the Au_4 tetrahedron configuration, while the interfacial binding energy E_b is -1.28 eV for the Au_4 upright configuration and -2.27 eV for the Au_4 tetrahedron configuration. For small neutral Au_n [$n < 12$ (Ref. 36)] clusters in the gas phase, 2D configurations are more stable than 3D configurations, and the reason was attributed to the relativistic effects.[66] This explains why the E_c of the 2D Au_4 upright configuration is more negative than that of the 3D Au_4 tetrahedron configuration. On the other hand, the Au_4 tetrahedron can be assumed to consist of three planar upright Au_3 clusters, and thus each of the interfacial Au atoms has similar interfacial reactivity with that of the Au_4 upright configuration. Note that the Au_4 tetrahedron has three interfacial Au atoms, whereas the Au_4 upright configuration has only two interfacial Au atoms. Therefore the interfacial binding energy E_b for the Au_4 tetrahedron is more negative than that of the Au_4 upright configuration. Combining the two aspects of cohesive energy E_c and binding energy E_b, we have the formation energy E_f of -7.24 eV for the Au_4 upright configuration and -7.15 eV for the Au_4 tetrahedron, and thus the Au_4 upright configuration is slightly more favorable than the Au_4 tetrahedron by 0.09 eV. With further increase of the size of Au clusters, since the 3D structure will have more reactive Au atoms than the upright one, the present calculations indicate that Au clusters on FeO/Pt(111) may transit to a 3D structure, for instance when $n > 4$.

In the gas phase the transition of an Au_n cluster from two to three dimensions is $n = 13$ for anion,[34] 8 for cation,[35] and 12 for neutral.[36] On perfect MgO(100) and anatase TiO_2(101), a 2D upright Au_n cluster is still preferred with n up to at least 7 and 6, respectively.[42] Given that a 2D upright Au_n cluster is stable on a perfect oxide when $n < n_c$ (where n_c is the critical atom number of Au clusters transiting from two to three dimensions), if $n_c < N_c$ (where N_c is the critical number in the gas phase), with the two effects of interfacial interaction and the intrinsic stability of the 2D configuration in gas phase in mind, then the transition of Au clusters from 2D to 3D Au_{n_c} should be accompanied by enhanced interfacial interaction from the increase of interfacial reactive Au atoms. Therefore, the reason for the earlier transition of Au clusters from the 2D upright to the 3D configuration on FeO/Pt(111) than on MgO

could be attributed to the stronger interfacial interaction of Au clusters with FeO/Pt(111) than with MgO(100).

IV. CONCLUSIONS

The adsorption of Au atoms and Au_2 and Au_4 clusters on FeO/Pt(111) have been studied by first-principles density functional theory. It was found that Au atoms binding with the lifted Fe cation of flipped adsorption are energetically favored throughout the Moiré superstructure of FeO/Pt(111), and Au atoms adsorbing directly on the oxygen layer are metastable or unstable. The process of Au lifting out the low-lying Fe cation is spontaneous in the HCP and Top domains, whereas there is a kinetic barrier in the FCC domain. The geometries of Au_2 and Au_4 clusters on FeO/Pt(111) have been explored and it was found that 1D (dimer) or 2D (Au_4) upright configurations are the most stable structures throughout the Moiré superstructure of FeO/Pt(111). Two effects, direction-dependent reactivity of planar Au clusters and electrostatic interfacial interaction, were found to be crucial in the configuration of Au clusters on oxide supports. Relativistic effects were found to be important for the configuration of Au clusters and interaction with FeO/Pt(111). These results highlight that the chemical state and geometry of Au clusters could be tuned by changing the oxide supports in one way or another, which could be used to improve the design of the catalysts.

ACKNOWLEDGMENTS

We are thankful for financial support from the Natural Science Foundation of China (Grant Nos. 20733008 and 20923001) and the Ministry of Science and Technology of China (Grant No. 2007CB815205).

*wxli@dicp.ac.cn

[1] N. Nilius, Surf. Sci. Rep. **64**, 595 (2009).
[2] F. P. Netzer, F. Allegretti, and S. Surnev, J. Vac. Sci. Technol. B **28**, 1 (2010).
[3] H.-J. Freund, Surf. Sci. **601**, 1438 (2007).
[4] H.-J. Freund, Chem. Eur. J. **16**, 9384 (2010).
[5] Q. Fu, W.-X. Li, Y. Yao, H. Liu, H.-Y. Su, D. Ma, X.-K. Gu, L. Chen, Z. Wang, H. Zhang, B. Wang, and X. Bao, Science **328**, 1141 (2010).
[6] H.-J. Shin, J. Jung, K. Motobayashi, S. Yanagisawa, Y. Morikawa, Y. Kim, and M. Kawai, Nat. Mater. **9**, 442 (2010).
[7] C. Harding, V. Habibpour, S. Kunz, A. N.-S. Farnbacher, U. Heiz, B. Yoon, and U. Landman, J. Am. Chem. Soc. **131**, 538 (2009).
[8] F. Claeyssens, C. L. Freeman, N. L. Allan, Y. Sun, M. N. R. Ashfold, and J. H. Harding, J. Mater. Chem. **15**, 139 (2005).
[9] C. Tusche, H. L. Meyerheim, and J. Kirschner, Phys. Rev. Lett. **99**, 026102 (2007).
[10] M. Kiguchi, S. Entani, K. Saiki, T. Goto, and A. Koma, Phys. Rev. B **68**, 115402 (2003).
[11] M. Xue and Q. Guo, J. Chem. Phys. **127**, 054705 (2007).
[12] M. Ritter, W. Ranke, and W. Weiss, Phys. Rev. B **57**, 7240 (1998).
[13] W. Ranke, M. Ritter, and W. Weiss, Phys. Rev. B **60**, 1527 (1999).
[14] G. Ketteler and W. Ranke, J. Phys. Chem. B **107**, 4320 (2003).
[15] N. A. Khan and C. Matranga, Surf. Sci. **602**, 932 (2008).
[16] C. Noguera, J. Phys. Condens. Matter **12**, R367 (2000).
[17] J. Goniakowski, F. Finocchi, and C. Noguera, Rep. Prog. Phys. **71**, 016501 (2008).
[18] J. Goniakowski, C. Noguera, and L. Giordano, Phys. Rev. Lett. **93**, 215702 (2004).
[19] J. Goniakowski, C. Noguera, and L. Giordano, Phys. Rev. Lett. **98**, 205701 (2007).
[20] X. Lin and N. Nilius, J. Phys. Chem. C **112**, 15325 (2008).
[21] N. Nilius, E. D. L. Rienks, H.-P. Rust, and H.-J. Freund, Phys. Rev. Lett. **95**, 066101 (2005).
[22] C. Lemire, R. Meyer, Sh. K. Shaikhutdinov, and H.-J. Freund, Surf. Sci. **552**, 27 (2004).
[23] M. Haruta, N. Yamada, T. Kobayashi, and S. Lijima, J. Catal. **115**, 301 (1989).
[24] M. Haruta, S. Tsubota, T. Kobayashi, H. Kageyama, M. J. Genet, and B. Delmon, J. Catal. **144**, 175 (1993).
[25] M. Haruta, CATTECH **6**, 102 (2002).
[26] M. Haruta, Nature (London) **437**, 1098 (2005).
[27] C. H. Christensen and J. K. Nørskov, Science **327**, 278 (2010).
[28] M. Valden, X. Lai, and D. W. Goodman, Science **281**, 1647 (1998).
[29] B. Yoon, H. Häkkinen, U. Landman, A. S. Wörz, J.-M. Antonietti, S. Abbet, K. Judai, and U. Heiz, Science **307**, 403 (2005).
[30] B. Hvolbæk, T. V. W. Janssens, B. S. Clausen, H. Falsig, C. H. Christensen, and J. K. Nørskov, Nano Today **2**, 14 (2007).
[31] Z.-P. Liu, X.-Q. Gong, J. Kohanoff, C. Sanchez, and P. Hu, Phys. Rev. Lett. **91**, 266102 (2003).
[32] M. Chen, Y. Cai, Z. Yan, and D. W. Goodman, J. Am. Chem. Soc. **128**, 6341 (2006).
[33] Y. Chen, P. Crawford, and P. Hu, Catal. Lett. **119**, 21 (2007).
[34] F. Furche, R. Ahlrichs, P. Weis, C. Jacob, S. Gilb, T. Bierweiler, and M. M. Kappes, J. Chem. Phys. **117**, 6982 (2002).
[35] S. Gilb, P. Weis, F. Furche, R. Ahlrichs, and M. M. Kappes, J. Chem. Phys. **116**, 4094 (2002).
[36] E. M. Fernández, J. M. Soler, I. L. Garzón, and L. C. Balbás, Phys. Rev. B **70**, 165403 (2004).
[37] I. Yudanov, G. Pacchioni, K. Neyman, and N. Rösch, J. Phys. Chem. B **101**, 2786 (1997).
[38] G. Barcaro and A. Fortunelli, J. Chem. Theory Comput. **1**, 972 (2005).
[39] S. Sicolo, L. Giordano, and G. Pacchioni, J. Phys. Chem. C **113**, 16694 (2009).
[40] R. Ferrando, G. Barcaro, and A. Fortunelli, Phys. Rev. B **83**, 045418 (2011).
[41] L. M. Molina and B. Hammer, J. Chem. Phys. **123**, 161104 (2005).
[42] L. M. Molina and J. A. Alonso, J. Phys. Chem. C **111**, 6668 (2007).
[43] S. Vajda, R. E. Winans, J. W. Elam, B. Lee, M. J. Pellin, S. Seifert, G. Y. Tikhonov, and N. A. Tomczyk, Top. Catal. **39**, 161 (2006).
[44] N. Cabrera and N. F. Mott, Rep. Prog. Phys. **12**, 163 (1949).
[45] G. Pacchioni, L. Giordano, and M. Baistrocchi, Phys. Rev. Lett. **94**, 226104 (2005).
[46] V. Simic-Milosevic, M. Heyde, N. Nilius, T. König, H.-P. Rust, M. Sterrer, T. Risse, H.-J. Freund, L. Giordano, and G. Pacchioni, J. Am. Chem. Soc. **130**, 7814 (2008).

[47]V. Simic-Milosevic, M. Heyde, X. Lin, T. König, H.-P. Rust, M. Sterrer, T. Risse, N. Nilius, H.-J. Freund, L. Giordano, and G. Pacchioni, Phys. Rev. B **78**, 235429 (2008).
[48]D. Ricci, A. Bongiorno, G. Pacchioni, and U. Landman, Phys. Rev. Lett. **97**, 036106 (2006).
[49]L. Giordano, G. Pacchioni, J. Goniakowski, N. Nilius, E. D. L. Rienks, and H.-J. Freund, Phys. Rev. Lett. **101**, 026102 (2008).
[50]J. Goniakowski, C. Noguera, L. Giordano, and G. Pacchioni, Phys. Rev. B **80**, 125403 (2009).
[51]G. Kresse and J. Furthmuller, Phys. Rev. B **54**, 11169 (1996).
[52]P. E. Blöchl, Phys. Rev. B **50**, 17953 (1994).
[53]G. Rollmann, A. Rohrbach, P. Entel, and J. Hafner, Phys. Rev. B **69**, 165107 (2004).
[54]L. Giordano, G. Pacchioni, J. Goniakowski, N. Nilius, E. D. L. Rienks, and H.-J. Freund, Phys. Rev. B **76**, 075416 (2007).
[55]J. P. Perdew, J. A. Chevary, S. H. Vosko, K. A. Jackson, M. R. Pederson, D. J. Singh, and C. Fiolhais, Phys. Rev. B **46**, 6671 (1992).
[56]G. Henkelman, B. P. Uberuaga, and H. Jónsson, J. Chem. Phys. **113**, 9901 (2000).
[57]L. R. Merte, J. Knudsen, L. C. Grabow, R. T. Vang, E. Lægsgaard, M. Marvikakis, and F. Besenbacher, Surf. Sci. **603**, L15 (2009).
[58]E. D. L. Rienks, N. Nilius, H.-P. Rust, and H.-J. Freund, Phys. Rev. B **71**, 241404(R) (2005).
[59]W. Zhang, Z. Li, Y. Luo, and J. Yang, J. Phys. Chem. C **113**, 8302 (2009).
[60]L. R. Merte, L. C. Grabow, G. Peng, J. Knudsen, H. Zeuthen, W. Kudernatsch, S. Porsgaard, E. Lægsgaard, M. Mavrikakis, and F. Besenbacher, J. Phys. Chem. C **115**, 2089 (2011).
[61]P. Pyykkö, Angew. Chem. Int. Ed. **41**, 3573 (2002).
[62]G. C. Bond, J. Mol. Catal. A: Chem. **156**, 1 (2000).
[63]Quantum-ESPRESSO is a community project for high-quality quantum-simulation software, based on density functional theory, and coordinated by Paolo Giannozzi. See [http://www.quantum-espresso.org and http://www.pwscf.org].
[64]D. Vanderbilt, Phys. Rev. B **41**, 7892 (1990).
[65]H. J. Monkhorst and J. D. Pack, Phys. Rev. B **13**, 5188 (1976).
[66]H. Häkkinen, M. Moseler, and U. Landman, Phys. Rev. Lett. **89**, 033401 (2002).